The Astronomical Journal, 160:221 (16pp), 2020 November https://doi.org/10.3847/1538-3881/abb375

The Separation and Hα Contrasts of Massive Accreting Planets in the Gaps of Transitional Disks: Predicted Hα Protoplanet Yields for Adaptive Optics Surveys

Laird M. Close
Department of Astronomy, University of Arizona, 933 N. Cherry Ave., Tucson, AZ 85718, USA; lclose@as.arizona.edu
Received 2020 June 10; revised 2020 August 21; accepted 2020 August 25; published 2020 October 27

Abstract

We present a massive accreting gap planet model that ensures large gaps in transitional disks are kept dust free by the scattering action of three coplanar quasi-circular planets in a 1:2:4 mean motion resonance (MMR). This model uses the constraint of the observed gap size, and the dust-free nature of the gap, to determine within ∼10% the possible orbits for three massive planets in an MMR. Calculated orbits are consistent with the observed orbits and Hα emission (the brightest line to observe these planets) for LkCa 15 b, PDS 70 b, and PDS 70 c within observational errors. Moreover, the model suggests that the scarcity of detected Hα planets is likely a selection effect of the current limitations of non-coronagraphic, low (<10%) Strehl, Hα imaging with adaptive optics (AO) systems used in past Hα surveys. We predict that as higher Strehl AO systems (with high-performance custom coronagraphs; like the 6.5 m Magellan Telescope MagAO-X system) are utilized at Hα, the number of detected gap planets will substantially increase by more than tenfold. For example, we show that >25 ± 5 new Hα "gap planets" are potentially discoverable by a survey of the best 19 transitional disks with MagAO-X. Detections of these accreting protoplanets will significantly improve our understanding of planet formation, planet growth and accretion, solar system architectures, and planet–disk interactions.

Unified Astronomy Thesaurus concepts: Planetary system formation (1257); Planet formation (1241); Protoplanetary disks (1300); Stellar accretion disks (1579); Exoplanet detection methods (489); Direct imaging (387); Circumstellar disks (235); Stellar accretion (1578); Accretion (14); Adaptive interferometry (19); Laser guide stars (904); Coronagraphic imaging (313)

Supporting material: machine-readable tables

1. Introduction

It is now well observationally established that some gas giant protoplanets, such as PDS 70 b and PDS 70 c, pass through a period of high luminosity as they accrete hydrogen gas from their circumplanetary disks producing detectable Hα emission. This was most clearly demonstrated in the direct detections of Hα emission from LkCa 15 b (Sallum et al. 2015), PDS 70 b (Wagner et al. 2018), and PDS 70 c (Haffert et al. 2019). Direct observations of protoplanets (defined here as accreting planets) are a key window into this poorly understood process of planet formation and accretion from a circumplanetary disk. While the exact mechanisms of planetary accretion are not yet fully understood, massive planets could magnetospherically accrete, via magnetic fields, directly onto the polar regions of the planet (Zhu et al. 2016; Thanathibodee et al. 2019 and references within).

1.1. A Lack of Hα Protoplanets?

Protoplanets can be difficult to discover since young, gas-rich, (<10 Myr) stars are $D > 120$ pc from Earth. Therefore, we must look to young stars with protoplanets on relatively rare wide (⩾10 au; ⩾80 mas) orbits. But how do we find such stars? Selection of optimal targets is facilitated by Atacama Large Millimeter/submillimeter Array (ALMA) dust continuum surveys like Disk Substructures at High Angular Resolution Project (DSHARP; Andrews et al. 2018), which have identified many young stars with transitional disks and wide disk gaps. For example, an exhaustive archival search of the ALMA archive by Francis & Van Der Marel (2020; hereafter FVDM) found 38 young stars with well-resolved wide 20–80 au gaps (see Figure 1). These dust-free gaps, or cavities, can be best explained by having multiple protoplanets clearing the gap. Dodson-Robinson & Salyk (2011) showed hydrodynamical simulations of a single planet at 10 au only being able to clear a ∼7 au wide gap (roughly ±4 Hill spheres), but three $3M_{\rm jup}$ "gap planets" inside a 20 au gap could maintain a dust-free gap.

In Section 2 we discuss the motivation for this study and add background information. In Section 3 we present a new "gap planet" model, and in Section 4 we project it onto nine of the most popular large-gap disks already observed with adaptive optics (AO) for Hα protoplanets. In Section 4 we also project our model onto all 23 large-gap transitional disks of FVDM. We use this model to predict what the detectable population of gap planets might be. In Section 5 we discuss these results and the potential success of more sensitive future Hα searches. In Section 6 we state our conclusions.

2. Motivation and Background

2.1. Reasons Protoplanets Might Be Faint at Hα—Or Is It All a Selection Effect?

As a result of the Very Large Telescope's (VLT) visible AO system (ZIMPOL) non-detections of new Hα planets (Cugno et al. 2019; Zurlo et al. 2020), there has been a series of papers describing why Hα planets might be apparently so rare. Brittain et al. (2020) suggest that planetary accretion could be episodic in nature, similar to an "FU Ori" type of outburst. Hence, it could be hard to catch the planets when they are near their peak of accretion/Hα luminosity. Brittain et al. (2020) suggest that PDS 70 b and c are in the middle between the quiescent and burst state. If either planet dramatically increases its Hα

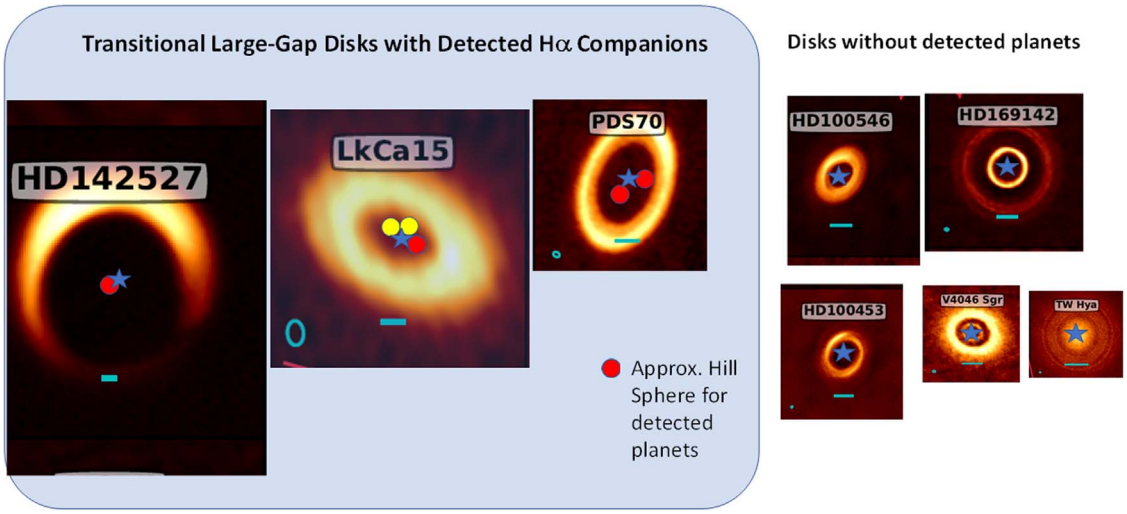

Figure 1. Big ALMA cavities yield gap planets. Early Hα spectral differential imaging (SDI) results include the exciting detections of HD142527B (Close et al. 2014), LkCa 15 b (Sallum et al. 2015), PDS 70 b (Wagner et al. 2018), and PDS 70 c (Haffert et al. 2019). These images are from ALMA, reproduced, with permission, from FVDM. We note that each image has been scaled so that the 30 au blue horizontal bar is the same size, highlighting correct relative sizes (except for HD142527, which is too large).

brightness in the future, this would prove the theory of Brittain et al. (2020). In another recent study, detailed three-dimensional thermo-hydrodynamical simulations of Szulagyi & Ercolano (2020) show that the extinction from dust could extinguish Hα from all but the most massive ($\geqslant 10 M_{\rm jup}$) planets. However, given that the masses of the PDS 70 c and b planets are $\sim$2 and $\sim$4 $M_{\rm jup}$, respectively (Wang et al. 2020a), then the dust-free "gas-only" models of Szulagyi & Ercolano (2020) are the only models in that study that can explain the observed properties and line strengths of PDS 70 b and c. In fact, a detailed physical model of magnetospherical accretion by Thanathibodee et al. (2019) shows that the accretion of PDS 70 b is well explained by magnetospherical accretion, but the efficiency of Hα line luminosity productivity falls dramatically if the mass accretion rate falls below a certain crossing point.

There is currently a tension in the literature as to how bright such "gap planets" should be at Hα. A key question that has not been rigorously poised or answered is: just how many of these Hα gap planets should we have detected already with current AO sensitivities? Are the null results (save for PDS 70 b, PDS 70 c, and LkCa 15 b) significant—or simply a selection effect of the limits of the AO surveys themselves? These AO systems cannot correct the atmosphere very well at Hα (656.3 nm is quite blue for AO correction; Close et al. 2018), particularly with fainter guide stars, since the coherence patch size ($r_{\rm o}$) of the atmosphere $r_{\rm o} = 15(\lambda/0.55)^{6/5}$ cm on a 0.″75 seeing night. Hence it is clear that $r_{\rm o}$ at the H band is 56 cm, but at Hα it is just 18 cm. So, only AO systems with $<$18 cm sampling of the telescope primary mirror will make the highest contrast images at Hα (see Close 2016 and Close et al. 2018 for reviews). For example, the Strehl of the corrected wave front may be 75% (residual wave front error 140 nm rms) at the H band (1656nm; where SPHERE was designed to work), but at Hα it is just 16%—so 84% of the starlight is outside of the diffraction point-spread function (PSF) and is swamping any Hα light from the planets. This simple scaling has another "hit" for Hα contrasts; the Strehls are so low that no coronagraph is used in any of the data sets of Cugno et al. (2019) and Zurlo et al. (2020). Hence the inner 0.″2 of the SPHERE/ZIMPOL images have 100% of the diffracted and atmospheric speckles swapping the individual images (making contrasts of $\leqslant 10^{-4}$ at 100 mas impossible). Similar limits apply to MagAO's Hα imaging as well (no coronagraph, low Strehls). All of these effects are not trivial and have made it difficult for MagAO to detect PDS 70 b even at 4σ and impossible for SPHERE/ZIMPOL for PDS 70 b (or c) at Hα (Wagner et al. 2018). The 4σ detection of PDS 70 b by MagAO was confirmed by the Very Large Telescope (VLT)/Multi Unit Spectroscopic Explorer (MUSE) by Haffert et al. (2019). But in all of these cases, the detections were difficult and required good correction on PDS 70, which is not a very bright guide star at $R \sim 11.8$ mag. Hence, it is fair to ask: is it a selection effect that, to date, most of the AO observed transitional disks are around the brightest targets, which, in turn, may very well be the "worst" targets since the high luminosity of the central stars drowns out the Hα planets? We first need a general predictive model of gap planet contrasts and separations to start to answer these valid questions about AO observational selection effects and planet yields.

In this paper we model a complete population of gap planet masses and orbits based purely on the physical characteristics of the ALMA observations of these transitional disks (size of gap, inclination of the gap, the stellar mass, and stellar R mag). The model creates a set of three planets in each of these large-gap disks that explains the dust-free gaps yet also remains dynamically stable $>$10 Myr. To model the Hα line luminosity of these planets, we then use a power-law break in the efficiency of Hα luminosity based on planetary mass accretion rates motivated by the physical planetary accretion models of Thanathibodee et al. (2019). We then derive relations between the brightness of the planet/star at Hα (Hα contrast, hereafter ΔmagHα), allowing for the prediction of the Hα contrast and the angular separation of a synthetic population of gap planets. Once this population is compared to average sensitivity curves from MagAO, SPHERE, and MUSE (all based on the detection sensitivity of real Hα planets), we can test whether the recent lack of detections proves that Hα planets are truly very faint. We may also find that there is a large population of gap planets that have not yet been discovered simply due to selection effects of the current surveys.

2.2. Current Approaches to Imaging Hα Planets

We can now make deep images with spatial resolutions of 20–25 mas (0.″025; Close et al. 2013, 2014; see review Close 2016; Close et al. 2018) from the ground at Hα. Previously, with the first large ⩾6.5 m visible AO system (MagAO), we achieved contrasts of 10^{-3} at 0.″2 from a bright star (Wagner et al. 2018) as we detected the in-fall of hydrogen gas as it accreted onto low-mass companions in the cleared gaps of transitional disks (Close et al. 2014; Sallum et al. 2015; Wagner et al. 2018; Haffert et al. 2019). All of these detections were made possible by the spectral differential imaging (SDI) technique where an Hα image has a scaled continuum image subtracted from it to remove some of the PSF speckles and reveal any Hα planets (Close et al. 2005, 2014).

2.3. New Hα Detection Techniques: Extreme Visible AO (MagAO-X) and MUSE

These impressive "Hα AO" detections were done with older AO systems (VLT/SPHERE, VLT/MUSE, Magellan/MagAO) with relatively low (<10%) Strehls at Hα. However, we have just had first light with the world's newest extreme AO system MagAO-X. MagAO-X is unique—it was designed from the start to work in the visible at high Strehl (Close et al. 2018; Males et al. 2018). MagAO-X yields a superior level of wave front control with a 2040 actuator Tweeter deformable mirror (DM) and a unique "extra" DM to eliminate all non-common path (NCP) errors between the science and wave front sensing (WFS) channels, minimizing coronagraphic leak. WFS with MagAO-X's very low noise (<0.6 rms e- read noise) electron multiplier charge-coupled device (EMCCD) pyramid WFS detector allows Strehls of 50% to be obtained while closed loop at 2 kHz (residual wavefront error (WFE) <120 nm rms—as demonstrated on-sky; J. R. Males et al. 2020, in preparation). The low noise of this sensor allows good correction even on faint $R \sim 13$ mag guide stars in good 0.″5 seeing conditions. The MagAO-X system with up to 1500 corrected modes maps to ∼15 cm/actuator, making it the highest sampled AO system in the world. Thus deeper, much more sensitive surveys for Hα planets are finally possible.

Two different approaches could lead to substantial increases in the number of Hα planets detected. For bright ($R < 12$ mag) targets, planets could be detected with MagAO-X and for those fainter ($R > 12$ mag) with the laser guide star fed VLT/MUSE Integral Field Unit (IFU). Hence, it is very important for the future of this field to know if the current lack of Hα detections is fundamental to the Hα line luminosity production (and extinction) mechanisms—or simply a result of selection effects in the current generation of AO surveys.

2.4. Past Successes Detecting Gap Protoplanets

2.4.1. The First Hα Planet: LkCa 15 b

It has been known for some time that there is a special class of circumstellar disk called a transitional disk. These disks have a lack of near-IR and mid-IR flux in their spectral energy distributions (Espaillat et al. 2007), which, when imaged by submillimeter interferometry, revealed large "gaps" (holes or cavities) in the dust distribution (see Figure 1). An excellent example of such a disk is that of LkCa 15 (Andrews et al. 2018). LkCa 15 had risen to importance since the speckle masking work on the 10 m Keck II telescope of Kraus & Ireland (2012) found evidence of a companion inside the large (∼72 au) gap transitional disk around LkCa 15. Later non-redundant masking work on the LBT telescope and re-reduction of the Keck data suggested that there were three objects in the LkCa 15 gap (Sallum et al. 2015) moving with a clear orbital motion over a 5 yr period. Simultaneously, yet independently of the LBT work, MagAO Hα observations found a 6σ Hα point source coincident with the NRM position for the LkCa 15 b planet on a 15 au orbit (0.″1) around LkCa 15 A. Only LkCa 15 b was detected in Hα. LkCa 15 (at decl. = +22° and $V \sim 12$) proved to be a challenging target from the south, and no subsequent MagAO data sets were of the same 0.″5 seeing quality of the published one. Recently Currie et al. (2019) have claimed that the NRM results could be due to bright dust clumps in the inner disk. However, FVDM find no evidence of significant inner dust in orbit around LkCa 15 in deep ALMA continuum images. Moreover recent high-resolution images from ALMA by Facchini et al. (2020) estimate that the compact optically thick central disk around LkCa 15 cannot be greater than ∼0.3 au. Hence these "clumps" (unseen by ALMA) could be compact and optically thick at submillimeter wavelengths and could, therefore, be compact circumplanetary disks around planets b and c. This would explain why the dust was difficult to detect by ALMA (Wu et al. 2017b). In any case, the observed strong Hα emission from LkCa 15 b cannot be explained by anything other than a protoplanet. However, LkCa 15 b still needs a significant detection at another epoch at Hα to be 100% unambiguous.

2.4.2. PDS 70 b and c

As Figure 1 shows, there are a handful of very large gaps known. It is interesting to note that in *every* case of a very wide gap, there was an accreting companion discovered inside the gap. An excellent example is the PDS 70 system. PDS 70 A is an $0.8 M_{\rm Sun}$ T Tauri star of age 5 Myr accreting at $\sim 6 \times 10^{-11} M_{\rm Sun}\,{\rm yr}^{-1}$ (Thanathibodee et al. 2020), which has a spectacularly large 74 au wide gap (see Figure 1). Imaging with SPHERE was able to discover thermal emission from the circumplanetary disk and atmosphere from the gap planet PDS 70 b (Keppler et al. 2018). We were able to use MagAO to discover Hα likely from magnetospherical accretion onto PDS 70 b (Wagner et al. 2018). The VLT's MUSE IFU was used to confirm the Hα emission from PDS 70 b and discovered PDS 70 c as another Hα protoplanet inside the gap (Haffert et al. 2019; see Figure 2). Since the separations of PDS 70 b and c are rather large (∼0.″19 and ∼0.″23, respectively), telescopes like Keck at L' (3.8 μm) are able to follow up with these planets to detect their circumplanetary disk emission (Eisner 2015) where the masses are measured to be roughly ~ 2–$4 M_{\rm jup}$ for b and ~ 1–$2 M_{\rm jup}$ for c (Wang et al. 2020a).

We caution that while L' is superior to Hα in piercing any dust extinction, it can be hard to achieve the required spatial resolutions at longer wavelengths. For example, PDS 70 b at 0.″185 translates to just 2.5 λ/D at L' with the large $D = 10$ m Keck telescope; this is very close to the inner working angle limit for high-contrast ($\sim 10^{-4}$) direct detection. Closer-in planets at, say, ∼0.″1 (1.3 λ/D at Keck) would really require an extremely large telescope–sized aperture for high-contrast direct direction at L'. In contrast, Hα is a 5.8× shorter wavelength, so even a smaller $D = 6.5$ m telescope finds a 0.″1 planet at 5 λ/D at Hα, and so it can be detected quite easily

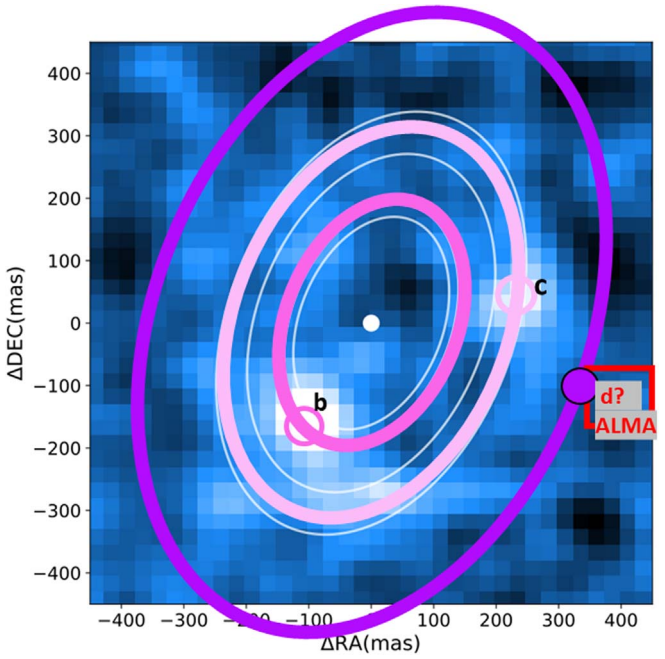

Figure 2. Hα image of PDS 70 b, c (Haffert et al. 2019). The predicted inner ($a_1 = 0.30Rcav$) and middle ($a_2 = 0.47Rcav$) orbits from our MAG model applied to the Rcav = 74 au PDS 70 cavity/gap. The open circles show the predicted planet positions (PA is fit to the planets); in excellent agreement with the observation. Planet "d" is hinted at by an ALMA detection (red box). We cannot detect outer planet d at Hα due to the disk's inclination (see red line in Figure 3).

(especially if a coronagraph is used), even if it is at 10^{-4} contrasts.

2.5. How Transitional Disks Can Maintain These Large Dust-free Gaps

In transitional disks, whose dust-cleared central cavities are optically thin, there is little extinction toward the protoplanet. This is especially true for the polar regions of the planet where the Hα is created by the shock from the magnetospherical accretion. In fact, it has been theorized that the reason these gaps stay dust free is due to the sculpting influence of giant planets (Alexander & Armitage 2009). The best gap planet candidate systems are the so-called "wide-gap" transitional disks that may need multiple >1 $M_{\rm jup}$ mass planets to keep the gap cleared, since these gaps are $\pm 4R_{\rm H}$ (Hill spheres). The size of any one planet's Hill sphere is approximately:

$$R_{\rm H} = (33/40)(a/10)(M_{\rm p}/M_{*})^{1/3}\ {\rm au}; \quad (1)$$

where $M_{\rm p}$ is the mass of the planet in $M_{\rm jup}$, and M_{*} is the mass of the star in solar masses. Hence even a massive 5 $M_{\rm jup}$ planet can only open a 10 ± 5 au dust-free gap at $a = 10$ au in 10 Myr (according to the hydrodynamical (HD) simulations of Dodson-Robinson & Salyk 2011, in agreement with the more recent 3D HD models of Sanchis et al. 2020). The popular "gap planets" theory of Dodson-Robinson & Salyk (2011) makes a convincing case that multiple (three), massive (3 $M_{\rm jup}$), coplanar gas planets can produce all of the commonly observed properties of transitional disks, including large gaps. Such gap planets scatter the dust creating the observed gaps but let the gas pass through the gap. Some gas accretes onto the planets, and the rest accretes onto the star. This allows for long-lived (>5 Myr) gaps around continuously accreting T Tauri stars. These timescales fit the observations (Figures 1 and 2) much better than the competitor "photoevaporation" theory, which states that once a large gap is cleared, the theory predicts that accretion onto the star quickly ends. There are too many large gaps over a large age range (1–10 Myr) for photoevaporation to explain all of these features (see the review of Owen 2016 and references within). But we should also be open to the question: if gap planets clear all of these cavities, why have we not observed Hα planets in *all* of these cavities (Brittain et al. 2020)? In the following sections, we attempt to address that question.

One thing appears clear: that in dust-free transitional disks, there should not be a large extinction along the observed line of sight to the planet (these are, after all, largely dust-free gaps). By targeting transitional disks that are not exactly edge-on (see Figure 1 for examples) we should be able to directly detect planetary Hα emission produced by gas accreting onto the planet (onto some shock surface/boundary) without high extinction along the line of sight. This exact point is proven by the 3D HD simulations of Sanchis et al. (2020) who find that once a significant gap is opened by a massive planet, the amount of residual dust leads to <1 mag of extinction toward the planet at the wavelength of Hα.

3. A New Model for Massive Accreting Gap Planets

3.1. The Massive Accreting Gap Model

The model of Dodson-Robinson & Salyk (2011; herein the DRS model) has continued to be the most common explanation for these large gaps in the literature. However, there are a few inconsistencies with observational data. For example, DRS predicts that all of the gap planets have the same mass, implying that all gap planets would be equally bright at Hα and other wavelengths. Imaged multi-planet systems are very rare (only three systems are known), yet there is a uniform trend that the outer planet is always lower in mass than the inner planets. For example, PDS 70 b (inner planet) is roughly two times the mass of outer planet PDS 70 c (Wang et al. 2020a). Similarly HR8799 c (middle planet) is roughly 1.4× the mass of HR8799 b (outer planet). Moreover, the mass of the inner planet HR87799 e is 1.4× the mass of HR8799 d (Marois et al. 2010; Currie et al. 2011). Moreover, the newest addition to this small list of wide multi-planet systems, TYC 8998-760-1, also has an inner planet 1.75× the mass of the outer planet (Bohn et al. 2020). So, there is a well observed steady trend of massive, wide, multi-planet systems increasing in mass approaching the innermost planet. Even in our own solar system, Saturn is 3.0× more massive than the combined mass of outer planets Uranus and Neptune, and Jupiter is 3.3× more massive than Saturn. Simply taking the average of these implies that the middle planet should be 1.4–3.0× more massive than the outer planet, and the inner planet should also be 1.4–3.0× more massive than the middle planet. To be consistent with this observed trend, we can average the above mass ratios (2.0, 1.4, 1.75, 3.0) = ⟨2.0⟩ and conclude that, on average, the middle planet is two times the mass of the outer planet, and the inner planet is two times more massive than the middle planet.

Also, the DRS model claims there must be a large massive planet within $4R_{\rm H}$ of the cavity edge (Rcav). In fact, detailed

modeling by Dong & Fung (2017) showed that disk-edge profiles (like those in Figure 1) showed signs of being sculpted by outer planets of masses no more than $\sim 1\,M_{\rm jup}$. This provides more observational evidence that the outer planet has a $\sim 3\times$ lower mass than that suggested by DRS.

Also, the long-term stability of the DRS model has been questionable past 10 Myr given that the planets were all massive but were not in a stable mean motion resonance (MMR). Nature prefers an MMR configuration for stability with massive planets. Our best example of a massive wide multi-planet system is the HR8799 e, d, c, b set of four massive (5–10 $M_{\rm jup}$) planets spanning over 70 au. We have been observing this system long enough to be able to fit HR8799 with a classic 1:2:4:8 MMR that allows for long-term stability (see Goździewski & Migaszewski 2014).

The PDS 70 b and c planets have been shown to be in a stable >1 Myr 1:2 MMR already in the 2D HD models of Bae et al. (2019). This gives us a strong indication that MMRs do play an important role in maintaining the long-term stability of having multiple massive planets inside large gaps. We can use the strong orbital relationship between planets in an MMR to synthesize a large population of gap planets that are each custom fit to the cavity they reside in. Recent *N*-body simulations of Wang et al. (2020b) show that in a gapped accretion disk it is possible that three massive gap planets are stable well past the disk dissipation time out to >10 Gyr if the planets are all very close to an MMR—near resonance but not perfectly locked into one. For a case of near-resonance orbits, the semimajor axes will be close enough to a perfect MMR that it will not significantly affect our massive accreting gap (MAG) model predicted separations on-sky. Thus, we adopt a perfect MMR for simplicity—while being cognizant that near-resonance systems would also look very similar and may be preferred in some cases by nature.

We can build on strengths of the DRS model with a new MAG model. In the MAG model we make two main assumptions. The first MAG assumption is that all three planets in the gap are in a stable 1:2:4 MMR,

$$a_2 = 2^{2/3} a_1;\ a_3 = 2^{2/3} a_2. \tag{2}$$

This is the most natural stable configuration for the system to evolve into as the planets all migrate inwards. Mechanisms of MMR formation are widely studied as the result of planetary migration (see a review by Papaloizou & Terquem 2006, and references therein). As soon as this migration starts, the planets open their individual gaps and then produce one large gap since their individual $4R_{\rm H}$ clearing zones overlap. At this point the inward migration nearly stops, and the orbits are stable and "locked" in the MMR (see, for example, Figure 3 of Goździewski & Migaszewski 2014). The second MAG assumption is that the mass of the inner planet is twice that of the middle planet, which, in turn is twice that of the outer planet ($M_{\rm p1} = 2M_{\rm p2} = 4M_{\rm p3}$) to be compatible with current observations as noted above.

To keep the gap edge (distance 1 *R*cav from star) dust free, we know that there must be 4 $R_{\rm H3}$ between that edge and location of the outer planet a_3. So,

$$R{\rm cav} - 4R_{\rm H3} = a_3, \quad \text{or} \quad R_{\rm H3} = (R{\rm cav} - a_3)/4. \tag{3}$$

For planet–planet stability, we require there to be 4.5 Hill spheres between the middle and outer planets (the mutual Hill spheres are also calculated for all of the planets in Table 1). Hence, if we need

Table 1
Orbits and Masses of MAG Planet Model

	Inner planet #1	Middle planet #2	Outer planet #3
Orbital semimajor axis (a) as fraction of disk gap (*R*cav)	0.300 *R*cav	0.475 *R*cav	0.753 *R*cav
a_2–a_1 in mutual Hill spheres	a_2–a_1 = 4.5 RH,m_{12}		
a_3–a_2 in mutual Hill spheres		a_3–a_2 = 5.6 RH,m_{23}	
Periods (1:2:4 MMR)	P_1	$2P_1$	$4P_1$
Planet mass ($M_{\rm p}$) in $M_{\rm jup}$(star mass (M_*) in solar units)	$3.96M_*$	$1.98M_*$	$0.99M_*$

there to be 4.5 $R_{\rm H3}$ between the middle and outer planets for stability, then from Equations (2) and (3), we can write:

$$a_3 - a_2 = a_3(1 - 2^{-2/3}) = 4.5\,R_{\rm H3} = 4.5(R{\rm cav} - {\rm a}_3)/4.$$

Solving the above for a_3 yields:

$$a_3 = \frac{R{\rm cav}}{1 + \frac{4}{4.5}[1\text{–}2^{-\frac{2}{3}}]} = 0.753R{\rm cav} \tag{4}$$

for all cavities in the MAG model. Applying Equation (4) to Equation (2) yields $a_2 = 0.475R$cav, and $a_1 = 0.300R$cav in the MMR.

There is, of course, a range of possible stable triple gap planet solutions, and we can explore their upper and lower bounds. The minimum value of a_3 for a stable solution is when the planet–planet distance is less than 4 $R_{\rm H3}$. So for the case where $a_{3\rm min}$–$a_2 = 4R_{\rm H3}$, then Equation (4) yields $a_{3\rm min} = 0.730$ *R*cav. On the other hand, the maximum $a_{3\rm max}$ is at the point that the planet–planet distance is $>8R_{\rm H3}$, at which point dust is no longer scattered away between the outer and middle planets (in this case the large gap would disappear and instead appear as a pair of narrow dust-free "rings" in ALMA imaging). From Equation (4) we find that if $a_{3\rm max}$–$a_2 = 8R_{\rm H3}$, then $a_{3\rm max} = 0.843R$cav. In summary, we see that the possible systematic error is $a_3 = 0.753^{+0.09}_{-0.02}$ *R*cav, $a_2 = 0.470^{+0.06}_{-0.01}$ *R*cav, and $a_1 = 0.300^{+0.03}_{-0.01}$ *R*cav. So the true semimajor axis could be as much as +12% to −3% with respect to the MAG values of a_3, a_2, and a_1. However, these errors are at the extrema, and so the likely error is well within 10%, which is an acceptable level of accuracy for the MAG model.

Since the outer planet is $4R_{\rm H3}$ from the edge of the gap (*R*cav), there must be a certain mass for the outer planet mass ($M_{\rm p3}$) to achieve this. We can see from Equations (3) and (1) that:

$$R_{\rm H3} = (R{\rm cav} - a_3)/4 = (33/40)(a_3/10)(M_{\rm p3}/M_*)^{1/3}\ {\rm au},$$

but substituting Equation (4) ($a_3 = 0.7525R$cav) and solving for M_{p3}/M_* yields:

$$\frac{M_{\rm p3}}{M_*} = \left[\frac{100(1 - 0.7525)}{33(0.7525)}\right]^3 = 0.99(M_{\rm jup}/{\rm M_{sun}}) \tag{5}$$

hence Equation (5) can be re-written as:

$$M_{\rm p3} = 0.99(M_*/M_{\rm sun}) \quad \text{in units of } M_{\rm jup}.$$

So, the more massive the star (M_*), the more massive the planets ($M_{\rm p}$). See Figure 3 for a cartoon of the MAG model,

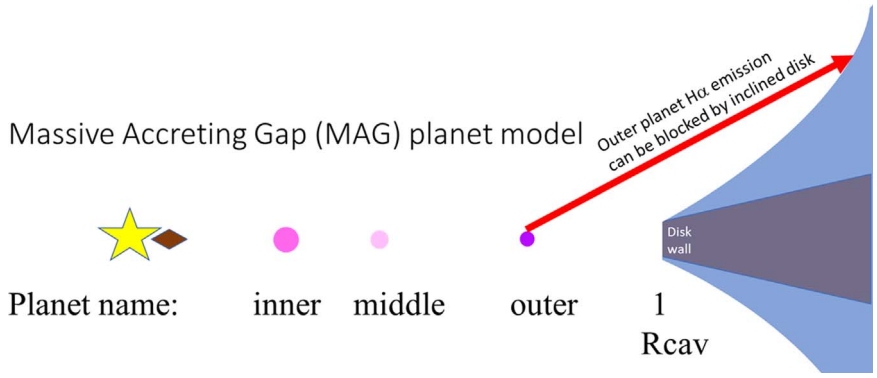

Figure 3. A cartoon of the MAG model of gap planets. This model satisfies the following conditions: (1) overlapping $\leqslant 4R_{\rm H}$ sectors to be dust free to *R*cav; (2) dynamically stable: 1:2:4 MMR; (3) each planet, pair-wise, has a separation of at least $2\sqrt{3}$ mutual Hill radii ($R_{\rm H,m}$); to be stable $\gg$10 Myr; and (4) the outer planet is located $4R_{\rm H3}$ from *R*cav to create dust-free edge. Planet size scales with mass.

and Table 1 for a summary of the model's parameters. It is important to note that the MAG model has no free parameters with respect to the orbits: the outer planet separation is simply given by:

$$\mathrm{sep}_3 = \frac{0.753R\mathrm{cav}}{D}\left[1 + \frac{2-\pi}{\pi}(1 - \cos(\mathrm{disk}_{\mathrm{inclination}}))\right] \quad \mathrm{arcsec} \quad (6)$$

where sep_3 is the average projected separation on-sky of the outer planet. We cannot, of course, know precisely the orbital phase (or position angle, PA) of the planet; only an average projection onto the sky can be predicted. But since the planets are co-orbital and co-aligned with the disk cavity, the projected orbits trace the cavity as projected on the sky. We can illustrate this by superimposing the predicted orbits from the MAG model onto the PDS 70 b and c system in Figure 2. We note that MAG's orbital calculations are consistent with the orbits of PDS 70 b and c (see Figure 2). For example, MAG predicts from PDS 70's 76 au gap that the inner planet ("b") should be at $0.3^{*}76 = 22.8$ au and the middle planet "c" at $0.475^{*}76 = 36.1$ au. Indeed, PDS 70 b is observed to be at 20^{+3}_{-4} au, and PDS 70 c is observed to be at 34^{+12}_{-6} au (Wang et al. 2020a); both are highly consistent with the MAG model calculated values. This gives a useful reality check of the MAG orbital predictions.

3.2. Hα Emission and Extinction in the MAG Model

How does the MAG model estimate the expected amount of Hα emission from a planet? The gas will "seek out" any gravitational potential wells (planets) on its slowly decaying orbit around the star—and these wells (planets) will emit in Hα as a fraction of the gas that magnetospherically accretes from the circumplanetary disk onto the high polar regions of the planets. A detailed physical model of this explains PDS 70 b's Hα emission in detail (Thanathibodee et al. 2019). This model predicts a mostly dust-free line of sight and significant Hα observed for the small ($\sim$2–4$M_{\rm jup}$) planets like PDS 70 c, b. This is in agreement with the 3D thermo-hydrodynamical models of Szulagyi & Ercolano (2020), but only in their "gas-only" case—this case best matches the observed properties of PDS 70 b, c.

Why are only "dust-free" models applicable to PDS 70 b and c? If any dust falls into the gap it is scattered by the outer planet, leaving the middle and inner planets almost completely dust free. This strongly suggests that the inner and middle planets should be best fit by the "gas-only" models of Szulagyi & Ercolano (2020), which explains why the Hα from PDS 70 b and c is detectable even though the masses of these planets are low.

3.3. Hα Line Luminosity Calculation by MAG Model: Example of PDS 70 b

As is already published in Section 3.4 of Close et al. (2014), the $L_{\rm H\alpha}$ luminosity can be calculated for a gap planet by comparing the flux with Vega in the usual manner:

$$L_{\rm H\alpha} = 4\pi D^2 \mathrm{vega}_{\mathrm{zero_{point}}} \Delta\lambda 10^{\frac{R\mathrm{mag-p-H\alpha}}{-2.5}}$$

where *R*mag_p_Hα is just the effective de-extincted "*R* magnitude" with respect to Vega for planet "b" at Hα (this is a good approximation since the center of the *R* filter, 658 nm, is almost exactly that of Hα, 656.3 nm). It is clear that *R*mag_p_Hα is equal to just the observed *R* mag of the star ($R_{\rm A}$) minus the extinction to both the star and the planet ($A_{\rm R}$). There is also the possibility that there is extra extinction toward the planet ($A_{\rm p}$) in addition to $A_{\rm R}$. There is also a slight correction for the leakage of the primary's continuum into *A*'s Hα measurement, which causes ΔmagHα to be slightly larger than it should be. This is an easy photometric correction to make via subtracting the star's magnitude at Hα from its continuum magnitude. Typically, the aperture flux of the primary in the Hα filter is $\sim$1.3× ($-$0.3 mag) that of the continuum (since the accreting star is also brighter at Hα than the continuum). There is also a very slight correction in the other direction since there is an extra $\sim$0.05 mag added due to Hα light in the *R* filter. So, the "*R* mag" of the planet is:

$$R\mathrm{mag\_p\_H\alpha} = (R_{\rm A}\text{-}A_{\rm R}) + (\Delta\mathrm{magH\alpha}\text{-}0.3 + 0.05) - A_{\rm p}.$$

In the case of PDS 70 b, we have very little extinction to the star ($A_{\rm R} \leqslant 0.2$ mag), and we assume $A_{\rm p}$ is zero (Wagner et al. 2018; Thanathibodee et al. 2019). Therefore, the line

luminosity $L_{H\alpha}$ can be written:

$$L_{H\alpha} = 4\pi D^2 \mathrm{Vega}_{\mathrm{zero_{point}}} \Delta\lambda 10^{\frac{R_A - A_R + \Delta\mathrm{magH}\alpha - 0.25 - A_p}{-2.5}}, \quad (7)$$

which we can directly solve for in the case of PDS 70 b as: $\mathrm{Log}(L_{H\alpha}/L_{\mathrm{Sun}}) = \log(4\pi(113^{*}3.1 \times 10^{18})^{2*}2.34 \times 10^{-5*}0.006/[3.9 \times 10^{33*}10^{((11.696-0.2+(7.36\pm0.47)-0.25)/2.5)}] = -5.70 \pm 0.19$ where the Vega zero-point magnitude in our Hα filter ($\mathrm{Vega}a_{\mathrm{zero\text{-}point}}$; see Males 2014 for the zero-point calibration of our $\Delta\lambda = 6$ nm wide Hα filter; or spectral resolution $R = 109$) is calculated to be 2.339×10^{-5} erg/(s cm^2 μm). This is a significant amount of emission and almost a 10× better contrast than at the *H* band (Keppler et al. 2018). We note that PDS 70 c is almost undetectable at the *H* band (Mesa et al. 2019), but quite detectable at Hα (Haffert et al. 2019) where it was discovered. Therefore, an SDI survey in Hα should be very sensitive to very low-mass gap planets that might be very difficult to detect at any other wavelength. The utility of Hα SDI to detect otherwise very faint gap planets was first predicted by Close et al. (2014).

Since low-mass, young objects have Xshooter calibrated accretions rates (Rigliaco et al. 2012), we can use:

$$L_{\mathrm{acc}} = 10^{[2.99\pm0.23+(1.49\pm0.07)*(\log(\mathrm{LH}\alpha))]}$$

from the empirical total accretion luminosity L_{acc} to $L_{H\alpha}$ relations of Rigliaco et al. (2012) for very low-mass accretors.

However, Thanathibodee et al. (2019) found, by applying the first full treatment of Hα line radiative transfer in a magnetospheric geometry for planetary-mass objects, that weakly accreting planets accreting with $\dot{M}_{\mathrm{p}} < 5 \times 10^{-12} M_{\mathrm{Sun}}\,\mathrm{yr}^{-1}$ (similar to PDS 70 c) are better fit with $\log(\dot{M}_{\mathrm{p}})$ varying as a $0.353\log(\mathrm{LH}\alpha)$ power law, so the production of Hα is less efficient. Hence, we find that in this case, this power law,

$$L_{\mathrm{acc}} = 10^{[-3.62+0.353\log(L\mathrm{H}\alpha)]}$$

better describes the relationship between Hα luminosity and total luminosity for low planetary accretion rates, which yields a lower accretion luminosity (L_{acc}). For example, in the case of PDS 70 b, the relationship yields $\log(L_{\mathrm{acc}}/L_{\mathrm{Sun}}) = -5.63 \pm 0.18$. Then using the standard relation for the released total accretion luminosity L_{acc} from accretion onto the planet surface

$$\dot{M}_{\mathrm{p}} = 1.25 L_{\mathrm{acc}} R_{\mathrm{p}}/(GM_{\mathrm{p}})$$

of Gullbring et al. (1998), we obtain a planetary accretion rate of $\dot{M}_{\mathrm{p}} = 5 \times 10^{-12}\,M_{\mathrm{Sun}}\,\mathrm{yr}^{-1}$ (using an M_{p} mass estimate of ∼4 M_{jup} for PDS 70 b; Wang et al. 2020a). Planet radii (R_{p}) are from 5 Myr COND evolutionary model estimate of $R_{\mathrm{p}} = 1.3R_{\mathrm{jup}}$ (Baraffe et al. 2003).

3.3.1. What Fraction of the Stellar Accretion Rate Accretes onto a Gap Planet in the Model?

The planetary accretion rate for PDS 70 b is 5×10^{-3} $M_{\mathrm{jup}}\,\mathrm{Myr}^{-1}$, which suggests the ∼5 Myr planet is at the end of its accretion phase. But even in this rather weak accretion flow, the Hα emission allowed both PDS 70 b and c to be detected. This planetary accretion rate is also equal to ∼10% of PDS 70 *A*'s stellar mass accretion rate $\dot{M}_{*} \sim 6 \times 10^{-11}\,M_{\mathrm{Sun}}\,\mathrm{yr}^{-1}$ (Thanathibodee et al. 2020). Therefore, we will adopt $f = 10\%$ as an estimate of the fraction (f) of the stellar accretion that is captured by a gap planet in the MAG model. For simplicity, we will assume this value holds for all MAG gap planets as a global average rate, although we are cognizant that this rate could vary between different planets and systems. However, we hope that, applied over a large number of systems, it will be helpful as a guide. Indeed, Lubow et al. (1999) predicted that the planetary gas capture rate could be as high as 50%; yet in the case of three planets, this would effectively cut off accretion to the star itself (leaving just <12%) and would also imply rapid planet growth to brown dwarf masses. Since stellar accretion is observed for all of our disk sample, and we removed any brown dwarf or stellar companions (eliminating binaries HD142527AB, GG Tau Ab, and V4046 Sgr AB), we will adopt that 10% of the stellar accretion is captured by each of the three gap planets ($f = 10\%$) in the MAG model.

Hashimoto et al. (2020) could not significantly detect PDS 70 b at Hβ with MUSE and claim that $A_{\mathrm{p}} \sim 2$ mag since Hβ/Hα < 0.3. They find $\dot{M}_{\mathrm{p}} = 5 \times 10^{-11}\,M_{\mathrm{Sun}}\,\mathrm{yr}^{-1}$, which is larger than the stellar $\dot{M}_{*}$ from *A*, suggesting $f > 100\%$. This very high f value is questionable since Hβ/Hα could be ∼0.3 for planets (with $Av = 0$), and also Hβ is very hard to measure as the Strehl at 486.1 nm is <4%; so b's weak Hβ is smeared out. Hence, we continue adopting $f = 10\%$ for the survey as a whole and for PDS 70 b and c.

4. Model Predictions

4.1. Model Predictions of the Hα Contrast of Gap Planets: Cases of High and Low Accretion

The MAG model can predict the planet/star contrast (Δmag at Hα) from the work above. For each planet there is a crossing point in the amount of the accretion flow onto that planet ($\dot{M}_{\mathrm{p}}$_cross) where accretion passes from being efficient to less efficient. In the high accretion case ($\dot{M}_{*} > 5 \times 10^{-11}$ $M_{\mathrm{Sun}}\,\mathrm{yr}^{-1}$), we can show from Equation (7) and the $L_{\mathrm{acc}} = 10^{[2.99\pm0.23+(1.49\pm0.07)*(\log(L\mathrm{H}\alpha))]}$ relations of Rigliaco et al. (2012) that (note that all terms are in standard astronomical cgs units, except D, which is in parsecs):

$$\Delta\mathrm{magH}\alpha = -1.675[\log M_{\mathrm{p}} + \log \dot{M}_{\mathrm{p}} - \log R_{\mathrm{p}}] + A_{\mathrm{R}} + A_{\mathrm{p}} - R_{\mathrm{A}} + 5\log D + 67.9, \quad (8)$$

but if weak accretion ($\dot{M}_{*} \leqslant 5 \times 10^{-11} M_{\mathrm{Sun}}\,\mathrm{yr}^{-1}$) then $L_{\mathrm{acc}} = 10^{[-3.62+0.353\log(L\mathrm{H}\alpha)]}$; so

$$\Delta\mathrm{magH}\alpha = -7.08[\log M_{\mathrm{p}} + \log \dot{M}_{\mathrm{p}} - \log R_{\mathrm{p}}] + A_{\mathrm{R}} + A_{\mathrm{p}} - R_{\mathrm{A}} + 5\log D + 258.22, \quad (9)$$

where M_{p} is the mass of the planet (from the MAG model), $\dot{M}_{\mathrm{p}} = f\dot{M}_{*}$ ($\dot{M}_{*}$ from FVDM), planet radius R_{p} is from the COND models, extinction toward the star A_{R} is from FVDM, the *R*-band (R_{A}) magnitude of the star is from SIMBAD, and the distance D (in parsecs) to the star is from FVDM. All of these observational inputs to Equations (8) and (9) are listed in Table 2.

The exact mass accretion rate at the crossing point when $\log(\dot{M}_{\mathrm{p}}) = \log(\dot{M}_{\mathrm{p}}\_\mathrm{cross})$ from the high luminosity (Equation (8)) to low luminosity (Equation (9)) case is linearly dependent on the planet radius and inversely dependent on planet mass. If we

Table 2
List of the Observed Parameters of the Large-gap Transitional Disks

Transitional disk system name	Log $\dot{M}_*$ ($M_{\rm Sun}$ yr^{-1})	$R_{\rm p3}$ ($R_{\rm jup}$)	$A_{\rm R}$ (mag)	$R_{\rm A}$ (mag)	D (pc)	$R_{\rm cav}$ (au)	M_* ($M_{\rm Sun}$)	L_* $L_{\rm Sun}$	Approx. inclination
HD 100453	∼−10.5	1.3	0.0	7.5	104	30	1.47	6.2	30°
HD 100546	−7.04	1.4	0.4	6.5	110	29	2.13	25	50
HD 135344B	−7.37	1.5	1.2	8.6	136	52	1.51	6.7	10
HD 169142	−8.7	1.4	0.4	8.3	114	26	1.65	8.0	0
LkCa 15	−8.4	1.6	1.2	11.61	159	72	1.32	1.3	50
MWC 758	−7.35	1.8	0.9	8.2	160	62	1.77	14	10
PDS 70	−10.22	1.3	0.2	11.71	113	76	0.8	0.3	49
UX Tau A	−7.95	1.7	1.6	9.83	140	33	1.4	2.5	40
V1247 Ori	−8.0	1.4	0.1	9.8	400	64	1.82	15	50
AA Tau	−8.44	1.3	2.4	11.0	137	44	0.68	1.1	60
AB Aur	−6.8	1.7	0.7	6.9	163	156	2.56	65.1	40
CQ Tau	∼−10.5	1.6	1.3	9.0	163	50	1.63	10	30
CS Cha	−8.3	1.6	1.0	11.1	176	37	1.4	1.9	20
DM Tau	−8.3	1.7	0.55	13.1	145	25	0.39	0.2	40
DoAr 44	−8.2	1.4	2.9	12.1	146	40	1.4	1.9	20
GM Aur	−8.3	1.6	0.3	11.7	160	40	1.01	1.0	60
HD 34282	∼−10.5	1.4	0.2	9.77	312	87	2.11	10.8	70
HD 97048	∼−10.5	1.5	0.9	8.3	185	63	2.17	30.0	60
HP Cha	−8.97	1.5	1.5	12.11	160	50	0.95	2.4	40
IP Tau	−8.14	1.7	1.45	12.46	131	25	0.54	0.6	60
RY Lup	−8.2	1.7	0.7	11	159	69	1.4	1.9	∼80
RY Tau	−7.1	1.7	2.2	9.67	175	27	2.25	15	∼80
T Cha	−8.4	1.4	2.0	12.75	107	34	1.12	1.3	∼80

Note. Table data is from FVDM unless otherwise noted in the text, except for $R_{\rm A}$, which is extrapolated from Simbad, the planet radius $R_{\rm p3}$ (from the COND models), and the disk inclination is estimated from the images of FVDM.

(This table is available in machine-readable form.)

rewrite the total accretion relation as

$$L_{\rm acc} = 10^{[b+(c)\log(L{\rm H}\alpha)]},$$

then we can derive an exact solution for the cross-over point from high accretion $L_{\rm acc}(b,c)$ to low accretion $L_{\rm acc}(b', c')$ as (in cgs units):

$$\log(\dot{M}_{\rm p}\_{\rm cross}) = \log(R_{\rm p}) - \log(M_{\rm p}) + (b'c - bc')/(c - c') + 40.86. \quad (10)$$

In the high efficiency case, $c = 1.49$ and $b = 2.99$ (Rigliaco et al. 2012), whereas in the lower efficiency case, $c' = 0.353$ and $b' = -3.62$ (adapted from Thanathibodee et al. 2019). So, from Equation (10):

$$\log(\dot{M}_{\rm p}\_{\rm cross}) = \log(R_{\rm p}) - \log(M_{\rm p}) + 35.19; \quad (11)$$

hence as $\dot{M}_{\rm p}$ falls below $\dot{M}_{\rm p}$_cross, there is a power-law break and decrease in the Hα flux.

Thus, we see from Equation (11), and Figure 4, that higher-mass planets can remain efficient at producing Hα ($\dot{M}_{\rm p} > \dot{M}_{\rm p}$_cross) compared to lower-mass planets since $\dot{M}_{\rm p}$_cross varies inversely with mass. For example, the first star in Table 2 is HD100453 for which the MAG model predicts a 5.66 $M_{\rm jup}$ inner planet. For that inner planet, $\log(\dot{M}_{\rm p}\_{\rm cross}_1) = -11.68$ (Equation (11)), which is just below the MAG estimated accretion rate of $\log(\dot{M}_{\rm p1}) = -11.5$ ($\dot{M}_{\rm p}$ estimated from 10% of the observed $\log(\dot{M}_*) = -10.5$ for this star; see Column 2 in Table 2). So since $\dot{M}_{\rm p1} > \dot{M}_{\rm p}\_{\rm cross}_1$, we can safely use Equation (8) to calculate ΔmagHα for HD100453's inner planet. However, the outer planet is predicted to have a mass that is four times lower, and as a result $\log(\dot{M}_{\rm p}\_{\rm cross}_3) = -11.08$. Since $\log(\dot{M}_{\rm p3}) = -11.5$ (again just 10% of $\dot{M}_*$), then we find $\dot{M}_{\rm p3} < \dot{M}_{\rm p}\_{\rm cross}_3$, and so we are in the lower luminosity case and we need to use Equation (9) to calculate ΔmagHα for HD100453's outer planet. Equation (11) allows, for every MAG planet in Table 3, its ΔmagHα to be correctly calculated by Equation (8), or if $\dot{M}_{\rm p} < \dot{M}_{\rm p}$_cross by Equation (9). In Table 3 we present all of the calculated gap planet properties calculated from the observed star/disk properties in Table 2. In Table 3 the values in bold text are cases where $\dot{M}_{\rm p} < \dot{M}_{\rm p}$_cross. As is clear from Table 3, usually $\dot{M}_{\rm p} > \dot{M}_{\rm p}$_cross since most of the transitional disks are accreting at much higher rates ("active accretors") than, for example, either PDS 70 or HD 100453, which are on the low end ("weak accretors").

4.1.1. The Special Cases of the Detected Hα Planets PDS 70 b, PDS 70 c, and LkCa 15 b

We can apply the MAG model to the known Hα planets. For LkCa 15 b we take the observed planet/star contrast (ΔmagHα) from the MagAO observations from Sallum et al. (2015). For PDS 70 we take the observed ΔmagHα from the MagAO observations by Wagner et al. (2018; MagAO observations are consistent with the filter width, and photometric zero-point used in Equation (7)) and the observed different between ΔmagHα of b and c from Haffert et al. (2019) from the MUSE IFU (since c has only been detected by the MUSE IFU at Hα). The results are presented in Figure 5. As can be seen from Figure 5, the model predicts Hα contrasts (ΔmagHα) consistent with observational errors. This is an

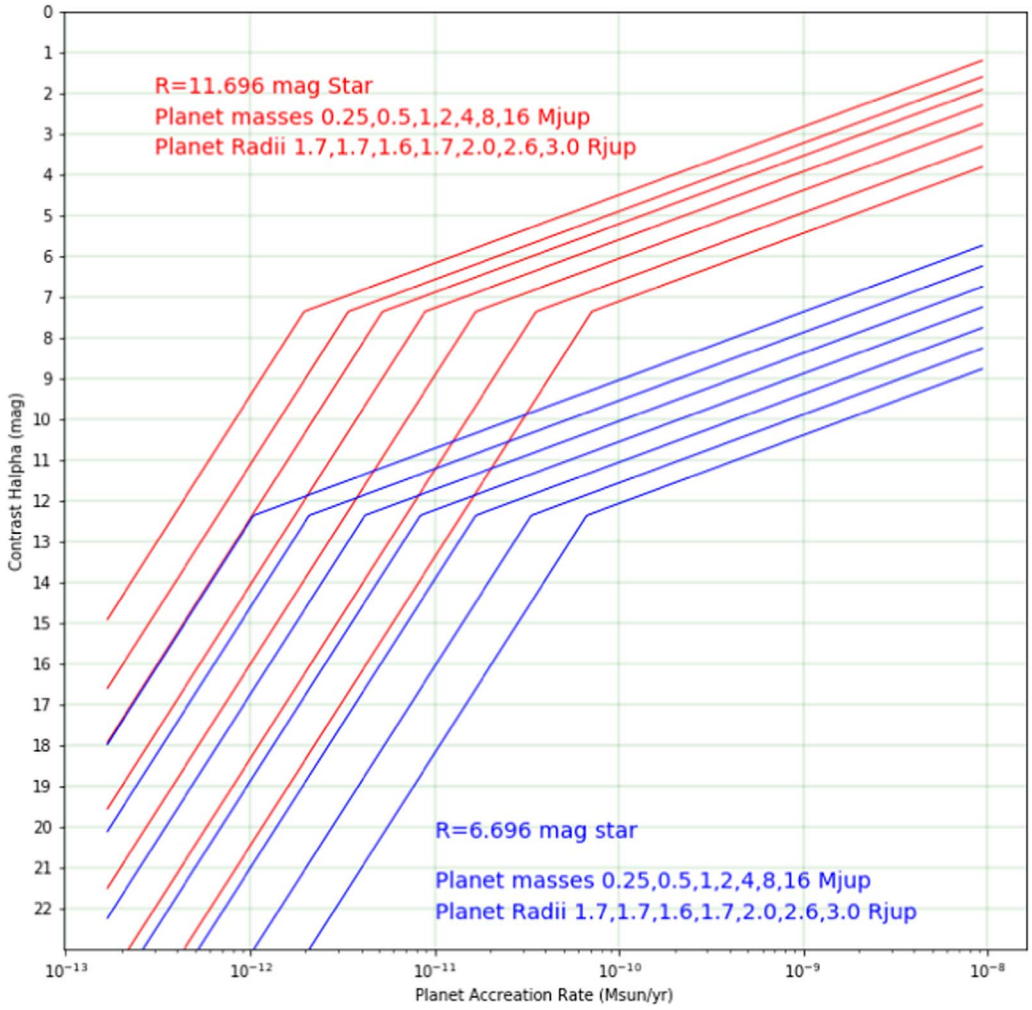

Figure 4. Plots of estimated ΔmagHα vs. $\dot{M}_{\rm p}$ from Equations (8) and (9). Note the sharp drop in Hα emission as $\dot{M}_{\rm p} < \dot{M}_{\rm p}$_cross (as the mass accretion rate onto the planet falls below the crossing point, and magnetospherical accretion is less efficient at generating Hα). We plot the contrasts from a 1 Myr old "faint" ($R = 11.696$ mag; like PDS 70 A) star in the top panel. The red lines are planet masses from 0.25 $M_{\rm jup}$ (lowest line) to 16 $M_{\rm jup}$ (highest line). All planet radii are from COND models. We also show the strong 100× increase in contrast required to detect the same population of planets around an otherwise identical "bright" ($R = 6.696$ mag) star. We illustrate here that the brightest, popular, AO stars can be poor (higher-contrast) targets for direct detection of Hα planets.

encouraging sign that the MAG model can reproduce all currently known gap planet Hα contrasts and orbits. The orbital fits are quite good, particularly in the case of PDS 70 b and c. In Figure 2 we overlay the predicted MAG orbits over the observed Hα planet positions, and the agreement is very good. This success encourages us to apply the MAG model to all nine of the previously observed large-gap disks that overlap between the FVDM and AO observations of Zurlo et al. (2020), plotted in Figure 6.

4.1.2. The MAG Model Applied to the Nine Most Commonly Observed Disks

It is straightforward to take the nine best (age <5 Myr; Rcav $>$ 20 au; highest $\dot{M}_{*}$) and most often AO observed Hα stars and predict which gap planets should have been detected and which are still too faint/close-in to be detectable with today's AO systems at Hα. This is done in Figure 6 where ΔmagHα versus separation is plotted for all stars in common between FVDM and Zurlo et al. (2020).

The most notable point of Figure 6 is that the top systems that are predicted to be most easily detected (PDS 70 and LkCa 15) have, in fact, *been* detected to have Hα gap planets. These planets are: PDS 70 b, c (Haffert et al. 2019) and LkCa 15 b (Sallum et al. 2015). This gives us some confidence in a reality check of the MAG model.

However, LkCa 15 c and d are predicted to also be detectable in the model, and indeed multi-epoch (5–7 yr) detections of point sources on Keplerian orbiting sources in Sallum et al. (2015) and Sallum et al. (2016) have been reported as c and d. However, neither of these candidates has been clearly detected at Hα. Recently LkCa 15 "c" and "d" have been suggested to be inner disk features (Currie et al. 2019), and so they may be compact dust and not gap planets. To be conservative we will not consider these planets as unambiguously detected. But we note that LkCa 15 b is a 6σ MagAO Hα source and hence a true gap protoplanet, and not a disk feature (Sallum et al. 2015); therefore it is used in this analysis. The true nature of the LkCa 15 c and d "objects" will hopefully be revealed by better AO correction in the near future. It is important to note that LkCa 15 at $R \sim 12$ mag and decl. $+24^{\rm o}$ is a very challenging AO target for today's Hα imagers in the Southern Hemisphere. The lack of a middle or outer Hα planet detection suggests that

Table 3
Predicted Planetary Parameters from the MAG Model of Gap Planets

	Orbital semimajor axis (au)			Average projected[a] separation on-sky (")			Planet/star contrast at ΔmagHα (mag)[b]			Predicted mass of planet (M_{jup})[b]		
Name	a_1	a_2	a_3	Sep_1	Sep_2	Sep_3	$\Delta H\alpha_1$	$\Delta H\alpha_2$	$\Delta H\alpha_3$	Mp_1	Mp_2	Mp_3
HD 100453	8.97	14.23	22.59	0.08	0.13	0.21	11.11	**11.61**	**12.12**	5.88	2.94	1.47
HD 100546	8.67	13.76	21.84	0.07	0.11	0.17	7.42	7.92	8.43	8.52	4.26	2.13
HD135344B	15.54	24.67	39.16	0.11	0.18	0.29	9.03	9.54	10.04	6.04	3.02	1.51
HD 169142	7.77	12.33	19.58	0.07	0.11	0.17	7.86	8.37	8.87	6.6	3.3	1.65
LkCa 15	21.52	34.16	54.22	0.12	0.19	0.30	5.50	6.00	6.51	5.28	2.64	1.32
MWC 758	18.53	29.41	46.69	0.11	0.18	0.29	8.87	9.37	9.88	7.08	3.54	1.77
PDS 70	22.71	36.05	57.23	0.18	0.28	0.45	7.25	**8.44**	**8.94**	3.20	1.6	0.80
UX Tau A	9.86	15.65	24.85	0.06	0.10	0.16	6.98	7.49	7.99	5.60	2.8	1.40
V1247 Ori	19.13	30.36	48.19	0.04	0.07	0.10	7.54	8.05	8.55	7.28	3.64	1.82
AA Tau	13.15	20.87	33.13	0.08	0.12	0.2	7.72	8.22	8.73	2.72	1.36	0.68
AB Aur	46.62	74.00	117.47	0.26	0.41	0.66	8.68	9.18	9.69	10.2	5.12	2.56
CQ Tau	14.94	23.72	37.65	0.09	0.14	0.22	11.96	**13.48**	**13.98**	6.52	3.26	1.63
CS Cha	11.06	17.55	27.86	0.06	0.1	0.15	6.15	6.66	7.16	5.60	2.8	1.40
DM Tau[c]	7.47	11.86	18.82	0.05	0.07	0.12	7.36[c]	7.86[c]	8.36[c]	1.56	0.78	0.39
DoAr 44[c]	11.95	18.98	30.12	0.08	0.13	0.20	8.58[c]	9.09[c]	9.59[c]	5.60	2.80	1.40
GM Aur	11.95	18.98	30.12	0.06	0.10	0.15	4.88	5.39	5.89	4.04	2.02	1.01
HD 34282	26.00	41.27	65.51	0.06	0.10	0.16	11.21	11.72	**12.09**	8.44	4.22	2.11
HD 97048	18.83	29.89	47.44	0.08	0.13	0.21	12.28	**12.68**	**13.04**	8.68	4.34	2.17
HP Cha[c]	14.94	23.72	37.65	0.09	0.14	0.21	8.79[c]	9.30[c]	9.80[c]	3.8	1.9	0.95
IP Tau[c]	7.47	11.86	18.82	0.05	0.07	0.12	7.07[c]	7.57[c]	8.08[c]	2.16	1.08	0.54
RY Lup	20.62	32.73	51.96	0.08	0.13	0.21	5.61	6.11	6.62	5.6	2.8	1.40
RY Tau	8.07	12.81	20.33	0.03	0.05	0.07	6.46	6.96	7.47	9.00	4.50	2.25
T Cha[c]	10.16	16.13	25.6	0.06	0.1	0.15	6.65[c]	7.16[c]	7.66[c]	4.48	2.24	1.12

Notes.
[a] We note that this is simply an average position; the true position on the sky depends on the unknown orbital phase, and so these separation values can underestimate the true separation by $(a/\pi D)(\pi - 2)(1 - \cos(\text{inclination}))$ and overestimate by $(a/D)[\cos(\text{inclination})–(1+((2 - \pi)/\pi)(1 - \cos(\text{inclination}))]$ arcsec.
[b] Assuming $Mp_1 = 2Mp_2$ and $Mp_2 = 2Mp_3$. The $\Delta H\alpha_1$ contrasts could have errors of up to 1.0 mag to −0.6 mag, and $\Delta H\alpha_2$ contrasts could have errors of +0.5 mag to −0.3 mag if the mass ratios vary from 1.4× to 3× instead of 2×. Also values of $\Delta H\alpha$ that are in boldface have been calculated with Equation (9), and all others have been calculated with Equation (8).
[c] Faint $R_A > 12$ mag AO targets have had their contrasts increased by +2 mag so they can be compared to the AO sensitivity limits in Figure 8. If they were observed above the Earth's atmosphere (or with an excellent laser guide star AO system), the contrasts listed above should be decreased by 2 mag.

(This table is available in machine-readable form.)

the innermost Hα planet might, in general, be easier to detect (the dust is scattered away by the outer planets, which, in turn, extinguishes the Hα from these planets).

Also, the MAG predicted outer planet "PDS 70 d" at ∼0.″43 has not been yet been definitively detected—even though it might have been just possible with MUSE. Keppler et al. (2019) have recently detected with ALMA a non-Keplerian (i.e., planet-like not primary disk-like; Pérez et al. 2014) ^{12}CO point source at 6σ. At 0.″39 it is near the 0.″43 MAG predicted position of PDS 70 d; moreover, at PA = 260°, the direct line of sight to "d" is blocked/extincted by the disk's 50° inclination, which explains why it is not a detected Hα source by MUSE in Figure 2. Further work with ALMA is required to confirm if this "d" object is real.

4.1.3. Extra Extinction to the Outer Planet and Cases of Dusty Gaps

In general, Hα from the outer planet can be blocked by an inclined disk (see the red arrow in Figure 3) or it is not easily detected against the glare of the disk "back wall" dust clumps. The inner two planets are less likely to be blocked by the flared disk, and they are much less likely to have any additional extinction as they are in the dust-free part of the disk gap. Thus the "gas-only" accretion case applies (Szulagyi & Ercolano 2020), leading to $A_{p1} \sim A_{p2} \sim 0$ mag. Therefore, outer planets can be the hardest gap planets to detect in Hα compared to the middle or inner planets (despite having a larger separation on-sky). Hence A_{p3} can be large, whereas A_{p1} and A_{p2} are likely close to zero. However, we do not know which outer planets are blocked by their flared disks (or dusty accretion flows; Szulagyi & Ercolano 2020), so we assume that A_{p3} is zero. However, the gaps of HD100546, HD135344B, MWC 758, and AB Aur are famous dusty spirals, and so to account for this extra gap dust, we adopt $A_p \sim 2A_R$ for each planet in these systems ($A_p \sim 0.8$–2.4 mag)—otherwise A_p is zero in Table 3.

Another interesting detail of Figure 6 is that MAG predicts only PDS 70 and LkCa 15 planets have wide and low enough contrast to be detected (purple circles above the dotted sensitivity curves). The other seven systems' planets are just a bit too tight/high-contrast to be detectable with today's Hα imagers. Since this is exactly what we observe, we can conclude that the MAG model has some predictive power. To discover more gap planets, we clearly need higher Hα contrasts at smaller separations.

4.2. Model Predictions for the Whole Population of Actively Accreting Large-gap Disks

We can also apply the MAG model to all 23 bright ($R <$ 13 mag) single stars from FVDM. It is likely that there are many possible gap planets that can be detected with slightly better contrast sensitivity at Hα. So, we need to understand

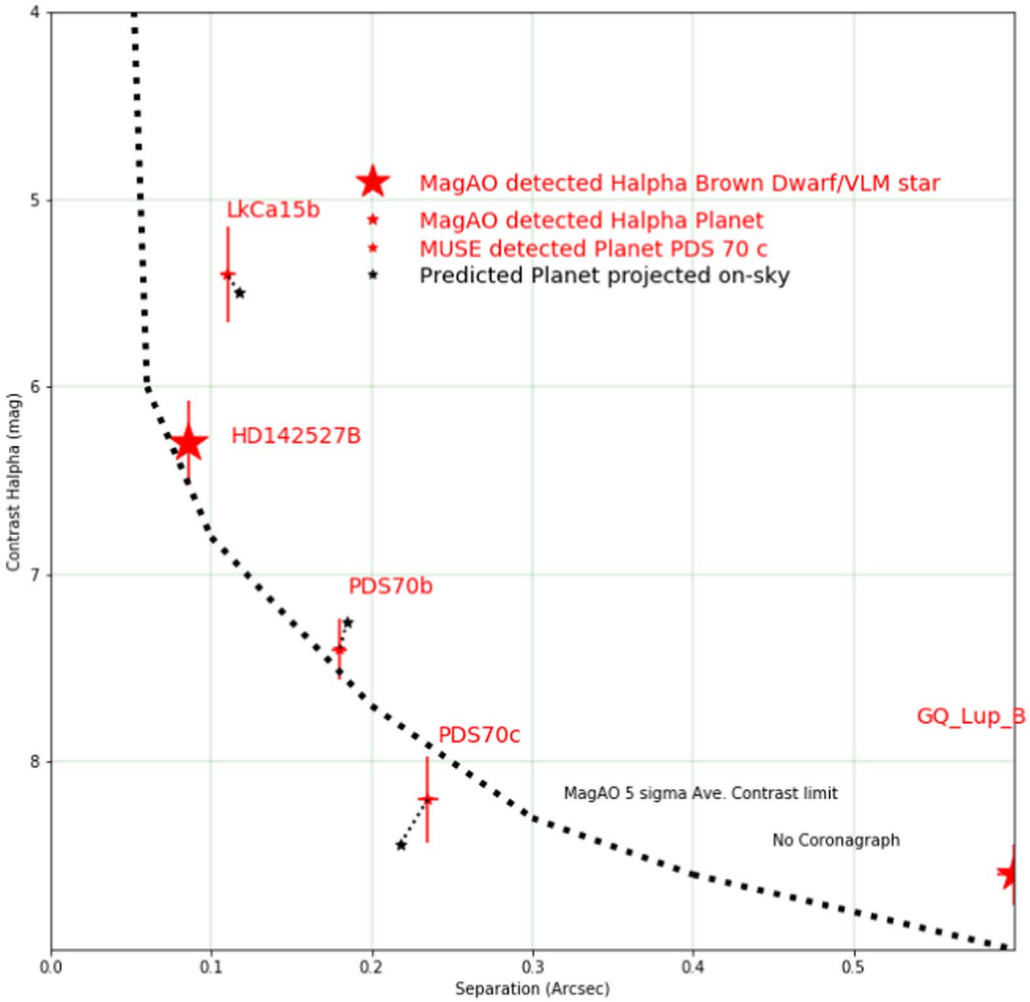

Figure 5. Fits of the MAG model to the previously detected Hα gap planets. Note how well the detectable planets (*small* red stars with error bars) are predicted by the MAG model (black stars) where the black star is corrected to the observed PA (orbital phase) of the planet it represents. Stellar companion HD142527B (Close et al. 2014) and brown dwarf GQ Lup B (Wu et al. 2017a) are also shown but are not fit by MAG. GQ Lup B is actually at 0.″8 but is shown here at the edge of plot for completeness.

what realistic contrasts might be like with advanced AO systems.

4.2.1. Contrast Curves for Future Surveys with MagAO-X

As we increase the number of controlled modes (∼1500), increase the speed >2 kHz, while simultaneously removing the read noise by use of EMCCD wave front sensors, the AO community is achieving higher and higher Strehls at Hα. MagAO-X with its impressive ∼15 cm/actuator mapping of the telescope pupil has been designed from the start for Hα planet imaging (Close et al. 2018; Males et al. 2018). MagAO-X had a successful first light in 2019 December. Results are reported in J. R. Males et al. (2020, in preparation). Here we will use the Hα contrast curves for MagAO-X from Males et al. (2019). These contrasts are based on full "end-to-end" models of the MagAO-X system. In Figure 7 we show a comparison of how PSF quality and contrasts at Hα can improve with MagAO-X. From these PSFs and full modeling of long 1 hr data sets with correct treatment of photon noise and residual speckle noise, we present the 1 hr contrasts of MagAO-X as the solid blue curve in Figure 8. This curve is consistent with the initial first light results of J. R. Males et al. (2020, in preparation).

4.2.2. How to Weight Contrasts for Faint and Bright AO Targets for the Same Plot

The five faintest targets are labeled with the blue colored text in Figure 8 ($12 < R_A < 13$ mag), and they each have their contrasts increased by 2.0 mag to account for the lower AO Strehls for these stars. These faint star observations could be executed in better than median observing conditions (good, slow, seeing); hence the blue curve is a good guide for all targets ($6 < R_A < 13$ mag) even if the contrasts will be ∼2.0 mag worse at $R_A \sim 13$ mag—because each faint "blue" target has had +2.0 mag added to the contrast in Figure 8 to compensate for this effect. This increase in contrast is reasonable because contrast scales as Strehl/(1-Strehl), and the Strehl is very low for these faint $R > 12$ targets. From space (or with an excellent laser guide star system), these targets would be quite promising since the Strehl loss would not apply, and these systems would have 2 mag smaller contrast than is shown in Figure 8.

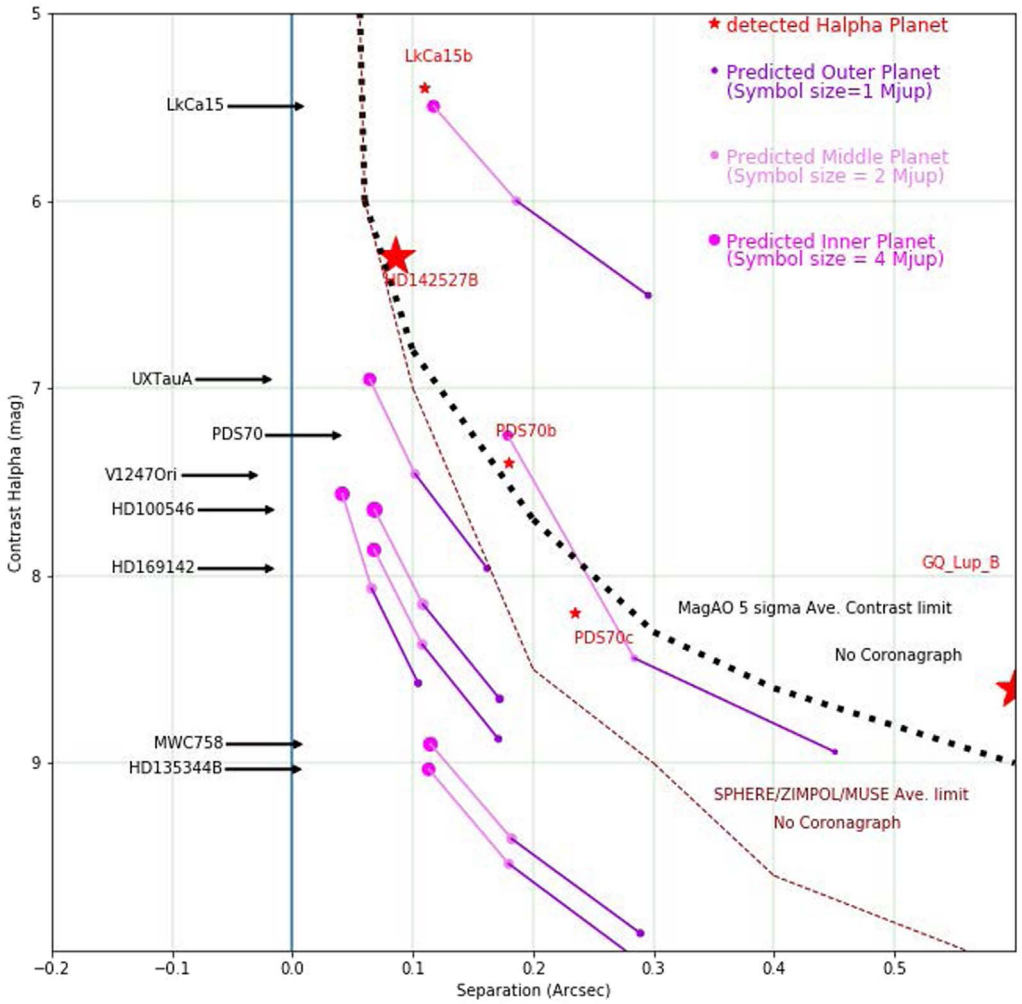

Figure 6. The MAG model applied to observed disks. LkCa 15 and PDS 70 appear as the best systems for Hα detections. All of the disks above have been observed by ZIMPOL, but no planets have been detected to date by these ZIMPOL observations (Cugno et al. 2019; Zurlo et al. 2020). To be a detectable planet at 5σ, a MAG gap planet (purple circles) must be above the dashed sensitivity curves. Current AO surveys are not quite sensitive enough to detect new Hα planets (other than in the PDS 70 and LkCa 15 systems). The ZIMPOL/MUSE average curve is from a 10th mag star (TW Hya) and similar to 8th mag stars HD 100546 and MWC 758 (Cugno et al. 2019). Although this average curve might be slightly too sensitive for fainter targets since ZIMPOL has yet to detect PDS 70 b, which is acceptable since it is just meant as an average sensitivity curve from $\sim 8 < R < 12$ mag.

5. Discussion

5.1. Some Famous Systems Not Included

5.1.1. Rings versus Wide Gaps in Transitional Disks: The Case of TW Hya

Figure 8 clearly shows that many disks look like excellent targets for future Hα observations. Right at the top (in terms of favorable ΔmagHα) would be a star that we did not include: TW Hya. TW Hya would be the oldest object in this list at $\sim$10 Myr. But it would also be the closest at 60 pc, which gives the self-luminous Hα from the planet a boost, and it is almost face-on. However, ALMA imaging of TW Hya does not show a very wide gap. It would be better described as a cleared narrow "ring." In the case of TW Hya, the ring is on the order of just $\sim$2 au wide (FVDM), so it must be cleared by a single gap planet at $a \sim 20$ au (so the three-planet MAG model does not apply). A single "ring" planet may suffer dust self-extinction, making detection at Hα problematic (Szulagyi & Ercolano 2020); hence TW Hya b may prove to be a difficult planet to detect at Hα. Such rings are quite common in ALMA high-resolution images, like those of DSHARP (Andrews et al. 2018). For example, the famous ALMA images of HL Tau show separate gaps or rings where three near-resonance massive planets can explain the observed gaps and have stable orbits >10 Gyr (Wang et al. 2020b), but those planets are each located in their own gap. Additionally, the *N*-body simulations of Wang et al. (2020b) do not consider all three planets in the same gap, yet they still argue that systems of three near-resonance massive planets can be stable in a gapped disk. However, a single massive planet can sometimes clear multiple rings (Zhang et al. 2018). But these rings are usually quite narrow, unlike the 20–80 au wide dust-free gaps that we list in Table 2, which each need multiple planets (Zhang et al. 2018). Hence, "ring" transitional disk systems are inappropriate for the MAG model. The MAG model only works for transitional disks with large dust-free gaps >20 au.

5.1.2. Circumbinary Rings versus Wide Gaps: HD 142527, GG Tau, and V4046 Sgr

We have tried to not include binaries because they do not require gap planets to clear their gaps since a single stellar companion will suffice (such as HD142527B; Close et al. 2014;

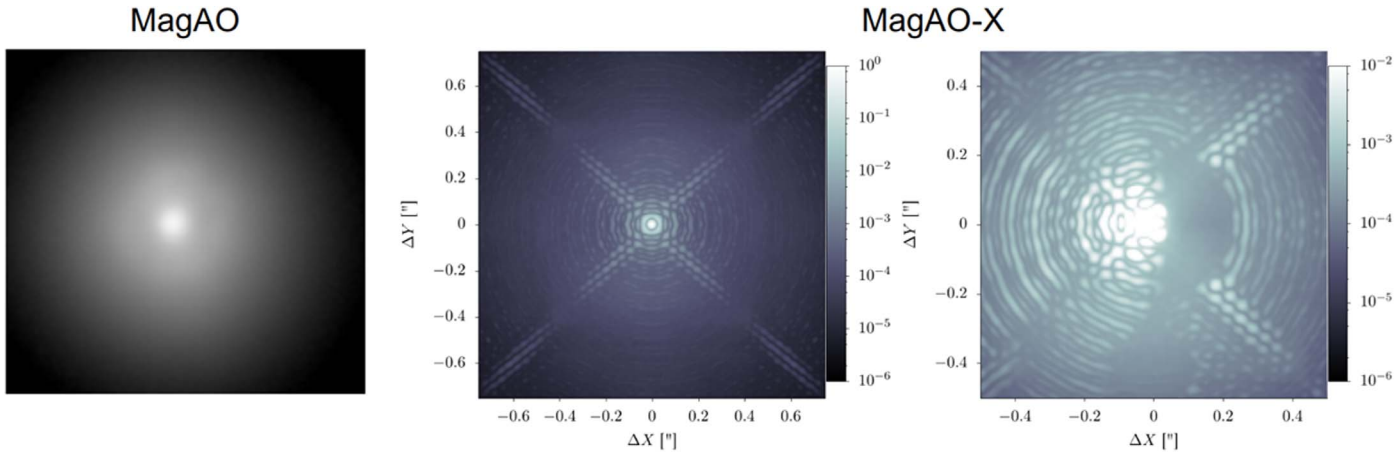

Figure 7. Improvements of Hα contrasts. MagAO (Strehl ~10%; no coronagraph) on an 11th mag star vs. simulated MagAO-X PSF on a 10th mag star in good seeing (50% Strehl). MagAO-X vAPP coronagraphic PSF to the far right. The raw contrasts are predicted to be $\sim 10^{-3}$ at 100 mas ($4.57\lambda/D$) with MagAO-X. After 1 hr and angular and spectral differential imaging (ASDI) with Karhunen-Loève Image Projection (KLIP) pipeline reductions (Males et al. 2014), the contrasts will approach 10^{-4} at 100 mas, and then 10^{-5} contrasts at 150 mas inside the "dark hole" (area of highest contrast to right of star) created by the interference effects of the vAPP (see solid blue line in Figure 8). This is a factor of $>100\times$ better contrast than what MagAO could achieve. Colors are raw PSF contrast.

or GG Tau Ab; Roddier et al. 1996). In the case of V4046 SgrAB, the binary is very tight and so may not be responsible for clearing the gap, and gap planets could be possibly present. However, the gap in V4046 is still a circumbinary disk and so is not appropriate for the MAG model.

5.2. Inclined Systems

In Figure 8 we can see some systems that look quite promising, including RY Lup, RY Tau, and T Cha. All of these systems have favorable predicted ΔmagHα, but we strongly caution here that they also have quite inclined disks (FVDM). Hence, any potential gap planets in these inclined systems may prove very difficult to detect at Hα due to dust extinction from their flared disks along the line of sight.

5.3. Low Accretors

Four disks (HD100453, CQTau, HD34282, and HD97048) did not have a single planet with ΔmagH$\alpha < 11$ mag. These stars have only upper limits ($<10^{-11}\,M_{\rm Sun}\,{\rm yr}^{-1}$) to the stellar mass accretion rate. Hence, there is not enough gas flow to produce a detectable amount of Hα from the planetary accretion. They were also hurt by the fact that their primaries were quite bright at ($R \sim$ 7–9th mag); clearly a gas-starved planet around a bright star is a poor Hα target, even if it is a good (bright) AO guide star (as shown by Figure 4).

This highlights another often overlooked bias in AO surveys where the brightest stars tend to be executed first (and best) since the AO correction is better and the observations are easier. However, as demonstrated in Figure 4, many of these bright stars need even higher contrasts to detect a planet—especially if there is little gas in the system. Hence, lower luminosity targets like PDS 70 and LkCa 15 (both with $R_{\rm A} \sim$ 11.7 mag) have relatively small ΔmagHα. These disks particularly become excellent targets when their very large (76, 72 au; respectively) gap sizes are also considered. Hence PDS 70 and LkCa 15 are the very best wide-gap planet targets in the sky.

5.4. The Southern Bias

It is also clear from comparing Figures 6–8 that there are many excellent targets that have not been observed yet at Hα with MagAO or VLT/SPHERE/ZIMPOL or MUSE. Some examples include AB Aur, GM Aur, and RY Tau. The reason that these have not been studied as closely at Hα is that, other than the 8 m Subaru's SCExAO system (Uyama et al. 2020), there are no high-contrast Hα imagers in the northern hemisphere, so these decl. $> +25^{\rm o}$ targets are challenging for southern AO systems. But Figure 8 suggests GM Aur and AB Aur could be excellent targets and worth the effort (while RY Tau suffers from a high inclination).

5.5. What Is the Expected Yield of a Future MagAO-X Survey?

From Figure 8 we predict with the MAG model a maximum yield of 48 ± 7 planets from 19 stars (44 would be new discoveries) in a future MagAO-X survey. This planet yield is robust; for example, a "flat" mass ratio model ($M_1 = M_2 = M_3$) applied to our sample would suggest a similar planet yield of ~43 planets. So, this prediction is not locked into the fine details of the MAG model alone.

In the future, advanced AO on the 25 m GMT (like GMagAO-X; Males et al. 2019; Close et al. 2020) or the 30 m TMT (like PSI; Fitzgerald et al. 2019) telescope will be able to detect all gap planets down to ~3 au orbits (Sallum et al. 2019).

5.6. What Is the Expected Yield of a Future Survey if the Outer Planets Are Not Detected?

It is possible that all of the outer planets prove hard to detect. This could be due to extinction by the disk edge (as could be the case for PDS 70 d), or due to higher intrinsic extinction ($A_{\rm p}$) due to the outer planet receiving the bulk of the infalling dust to scatter, or simply because there are only two massive (inner + middle) planets, and the outer planet is much less massive. Whatever the cause, we can see from Figure 8 that we still have 25 ± 5 new inner and middle planets detected even if outer planets are hard to detect. So, such a future survey will be productive regardless of the fine details of the true gap planet population.

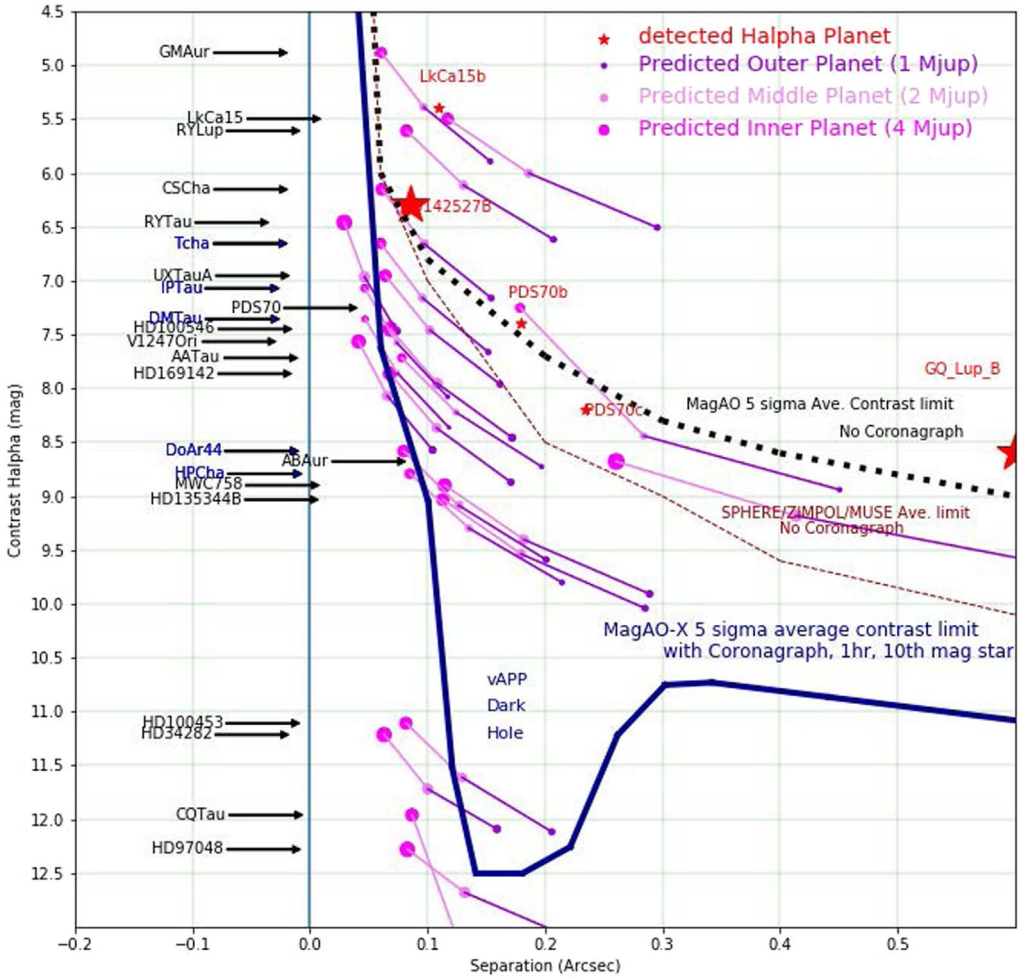

Figure 8. The MAG planet model applied to all 23 bright ($I < 13$) FVDM single stars. The MagAO-X 1 hr contrast limits from processing the images in Figure 6 are plotted as the solid blue line. We can trivially see that MagAO-X should be able to detect ~48 gap planets (44 new) from the top 19 systems (all those above HD100453).

5.7. Sensitively of the Predicted Planet Yields to Assumptions About the Planet Masses

The MAG model makes two main assumptions. One that the three planets are on an MMR spaced correctly so that the gap is cleared. This is a reasonable assumption based on stability of multi-planet wide systems like HR 8799bcde. The second is that the middle planet is two times the mass of the outer planet, and the inner planet is two times that of the middle planet ($M_{p1} = 2M_{p2} = 4M_{p3}$). This assumption is inspired by observations of all known wide multi-planet systems (PDS 70, HR 8799, TYC 8998-760-1, and even that of our own solar system). However, it could easily be that the mass ratio, instead of two times, is in the range of one to three times. In the case that the mass ratio is 1.0× (all planets same mass as M_3), this would have no effect on $\Delta\text{magH}\alpha_3$, but $\Delta\text{magH}\alpha_2$ would be +0.5 mag worse (bigger), and $\Delta\text{magH}\alpha_1$ would be +1.0 mag worse than that shown in Figure 8. On the other hand, if the mass ratio increased to three times (as in our solar system), then $M_{p2} = 3M_{p3}$ and $M_{p1} = 3M_{p2}$. In that case, $\Delta\text{magH}\alpha_3$ would still be the same, but $\Delta\text{magH}\alpha_2$ would be 0.3 mag better (smaller), and $\Delta\text{magH}\alpha_1$ would be 0.59 mag better (smaller). In other words, allowing for a wide range of mass ratios would not affect the $\Delta\text{magH}\alpha_3$ values, but it could change $\Delta\text{magH}\alpha_2$ by −0.3 to +0.5 mag and $\Delta\text{magH}\alpha_1$ by −0.59 to 1.0 mag compared to those values in Figure 8. While these are significant differences, they do not significantly affect the planet yields or major conclusions of this study. For example, the planet yield in the "worst case" for all of the planets with the same mass as M_{p3} ($M_{p1} = M_{p2} = M_{p3}$) is 42 systems of the 19 best stars (quite consistent with the 48 ± 7 found with the default $M_{p1} = 2M_{p2} = 4M_{p3}$). Hence, the MAG model's predicted planet yields are not highly sensitive to exact planet mass ratios. But it would be healthy to consider a possible range of −0.59 to +1.0 mag systematic error in our predictions of $\Delta\text{magH}\alpha_1$ to cover for possible mass errors of overestimating M_1 by four times and also for possibly underestimating M_1 by $9/4\times$. Similarly, the systematic errors of $\Delta\text{magH}\alpha_2$ could be as high as −0.3 to +0.5 mag. But neither of these error ranges significantly changes the planet yields.

It is certainly true that there will be a range of mass ratios in nature, and we do not expect the MAG model's $M_{p1} = 2M_{p2} = 4M_{p3}$ to hold for every system; at best it might prove to be an average relation over all systems. However, as noted above, the predicted planet yields are consistent with 48 ± 7 from $M_{p1} = M_{p2} = M_{p3}$ to $M_{p1} = 3M_{p2} = 9M_{p3}$. Hence, we do not consider the exact planet mass ratio relation to have to be known, a priori, to be able to estimate planet yields with the MAG model.

5.8. What Would a Null Result Mean for a Future Deep Hα Planet Survey?

Even in the *very* unlikely case that LkCa 15 b and PDS 70 b, c are the only gap planets detectable at Hα in nature (hence a future survey "null result"), the great sensitivity of MagAO-X to low-mass planets will allow astronomers to place tighter constraints on the outer extrasolar population than ever before (for both "cold-start" and "hot-start" planets; at Hα both are equally visible; Sanchis et al. 2020)—and such a "null" result would then reject the MAG and DRS multi-planet clearing gap models at $\sim 5\sigma$ significance. A future survey null result could also suggest that planetary accretion could be quite time variable (like FU Ori; Brittain et al. 2020), or that Hα produced by planetary accretion is heavily extincted, as suggested by the dusty models of Szulagyi & Ercolano (2020), and the low extinction toward PDS 70 b, c and LkCa 15 b was an outlier. However, we strongly suspect that PDS 70 b, c and LkCa 15 b are not the only Hα planets, and that future higher-contrast surveys will discover many more Hα planets (but these new planets will typically be higher-contrast, and closer-in, than the PDS 70 planets).

5.9. Future Theoretical Work for the MAG Model

The MAG model presented here is a very simple model that can predict the rough properties of planets clearing the gaps of wide transitional disks. While these gap planet MMRs can be stable for millions of years (as shown by the detailed 2D HD simulations of Bae et al. 2019 in the case of PDS 70 b and c), future detailed simulations considering both orbital migration and mass growth would will help inform the full history of these gap planets' orbital evolutions. For example, can they stay dynamically stable through phases of high rates of planet growth? In particular, it would be interesting to model in detail how the trapping of the planets into the MMR occurs during the slow orbital migration inwards (or outwards; Bae et al. 2019) for all of the accreting planets. During that period the planets must avoid: orbital instabilities, exciting the eccentricities, and close interactions between the planets. While this has been shown to work in the past (DRS model; Bae et al. 2019; Goździewski & Migaszewski 2014), more long-term evolutionary HD simulations with planetary accretion would be illuminating.

6. Conclusions

Submillimeter interferometry (Submillimeter Array, ALMA, etc.) has detected a significant group of large (20–80 au) gaps in many transitional disks (FVDM, references within). A handful of these disks has been shown to have Hα bright companions inside them (HD142527B; Close et al. 2014; LkCa 15 b; Sallum et al. 2015; PDS 70 b; Wagner et al. 2018; PDS 70 c; Haffert et al. 2019), but some transitional disk AO surveys have not revealed any new gap planets (Cugno et al. 2019; Zurlo et al. 2020). This has encouraged recent theoretical studies that suggest that Hα can be only detected from the most massive planets ($>10\ M_{\rm jup}$; Szulagyi & Ercolano 2020) or can be highly variable (Brittain et al. 2020). But are these null results a selection effect of the AO sample selected and the limits of high-contrast AO at Hα? To answer this question requires a simulated parent population of gap planets applied to all known wide-gap transitional disks.

We have presented an MAG planet model that ensures these large gaps are kept dust free by the scattering action of three coplanar planets in a 1:2:4 MMR. With few free parameters, our model is consistent with the observed separations and Hα fluxes of LkCa 15 b, PDS 70 b, and PDS 70 c within observational errors. Moreover, the model suggests that the scarcity of detected Hα planets is likely a selection effect of the current contrast limitations of non-coronagraphic, low Strehl, Hα imaging with older AO systems. We predict that, as higher Strehl AO systems (with high-performance custom coronagraphs; like MagAO-X) are utilized at Hα, the number of detected gap planets will substantially increase by, as much as, tenfold. Detections of a large number (∼25–44) of new accreting protoplanets will significantly improve our understanding of planet formation, solar system architectures, and planet–disk interactions.

We would like to thank the anonymous referee for many helpful suggestions that lead to a much improved manuscript. We would like to thank Jared Males for allowing Figure 11 from the MagAO-X PDR (Males et al. 2019) to be reproduced here and for helpful discussions. We thank Logan Francis and Nienke van der Marel for permission to reproduce their ALMA images in Figure 1. We would also like to thank Sebastiaan Haffert and Alycia Weinberger for helpful discussions about planetary accretion. We thank Kate Follette for helpful discussions about gap planets and their environments. L.C. was supported by a NASA eXoplanet Research Program (XRP) grant 80NSSC18K0441.

Facility: Magellan:Clay (MagAO); Magellan:Clay (MagAO-X).

ORCID iDs

Laird M. Close https://orcid.org/0000-0002-2167-8246

References

Alexander, R. D., & Armitage, P. J. 2009, ApJ, 704, 989
Andrews, S., Huang, J., Pérez, L. M., et al. 2018, ApJL, 869, L41
Andrews, S., Wilner, D., Espaillat, C., et al. 2011, ApJ, 732, 42
Bae, Jaehan, Zhu, Zhaohuan, Baruteau, Clément, et al. 2019, ApJL, 884, L41
Baraffe, I., Chabrier, G., Barman, T. S., Allard, F., & Hauschildt, P. H. 2003, A&A, 402, 701
Bohn, A., Kenworthy, M. A., Ginski, C., et al. 2020, ApJL, 898, 1
Brittain, S. D., Najita, J. R., Dong, R., & Zhu, Z. 2020, ApJ, 895, 48
Close, L. M. 2016, Proc. SPIE, 9909, 99091E
Close, L. M., Follette, K. B., Males, J. R., et al. 2014, ApJL, 781, L30
Close, L. M., Lenzen, R., Guirado, J. C., et al. 2005, Natur, 433, 286
Close, L. M., Males, J., Hedglen, A., et al. 2020, arXiv:2004.06808
Close, L. M., Males, J. R., Durney, O., et al. 2018, Proc. SPIE, 10703, 107034Y
Close, L. M., Males, J. R., Morzinski, K., et al. 2013, ApJ, 774, 94
Cugno, G., Quanz, S. P., Hunziker, S., et al. 2019, A&A, 622, 156
Currie, T., Burrows, A., & Itoh, Y. 2011, ApJ, 729, 128
Currie, T., Marois, C., Cieza, L., et al. 2019, ApJL, 877, L3
Dodson-Robinson, S., & Salyk, C. 2011, ApJ, 738, 131
Dong, R., & Fung, J. 2017, ApJ, 835, 146
Eisner, J. A. 2015, ApJ, 803, 4
Espaillat, C., Calvet, N., D'Alessio, P., et al. 2007, ApJL, 671, L135
Facchini, S., Benisty, M., Bae, J., et al. 2020, A&A, 639, A121
Fitzgerald, M., Bailey, V., Baranec, C., et al. 2019, BAAS, 51, 251
Francis, L., & van der Marel, N. (FVDM) 2020, ApJ, 892, 111
GoŸdziewski, K., & Migaszewski, C. 2014, MNRAS, 440, 3140
Gullbring, E., Hartmann, L., Briceno, C., & Calvet, N. 1998, ApJ, 492, 323
Haffert, S. Y., Bohn, A. J., de Boer, J., et al. 2019, NatAs, 3, 749
Hashimoto, J., Aoyama, Y., Konishi, M., et al. 2020, AJ, 159, 222
Keppler, M., Benisty, M., Müller, A., et al. 2018, A&A, 617, A44

Keppler, M., Teague, R., Bae, J., et al. 2019, A&A, 625, A118
Kraus, A. L., & Ireland, M. J. 2012, ApJ, 745, 5
Lubow, S. H., Seibert, M., Artymowicz, P., et al. 1999, ApJ, 526, 1001
Males, J., Close, L., & Guyon, O. 2019, BAAS, 51, 236
Males, J. R. 2014, MagAO-X PDR Simulation Document, 4.1 AO Control and Simulations, https://magao-x.org/docs/handbook/_downloads/65fb02fc185f5dac8bb0cddd5c55b755/4.1_simulations.pdf
Males, J. R., Close, L. M., Miller, K., et al. 2018, Proc. SPIE, 10703, 14
Males, J. R., Close, L. M., Morzinski, K. M., et al. 2014, ApJ, 786, 32
Marois, C., Zuckerman, B., Konopacky, Q. M., Macintosh, B., & Barman, T. 2010, Natur, 468, 1080
Mesa, D., Keppler, M., Cantalloube, F., et al. 2019, A&A, 632, A25
Muzerolle, J., Hillenbrand, L., Calvet, N., Briceño, C., & Hartmann, L. 2003, ApJ, 592, 266
Owen, J. E. 2016, PASA, 33, 5
Papaloizou, J. C. B., & Terquem, C. 2006, RPPh, 69, 119
Pérez, L. M., Isella, A., Carpenter, J. M., et al. 2014, ApJL, 783, L13
Rigliaco, E., Natta, A., Testi, L., et al. 2012, A&A, 548, A56
Roddier, C., Roddier, F., Northcott, M. J., Graves, J. E., & Jim, K. 1996, ApJ, 463, 326
Sallum, S., Bailey, V., Bernstein, R. A., et al. 2019, BAAS, 51, 527
Sallum, S., Eisner, J., Close, L. M., et al. 2016, Proc. SPIE, 9907, 99070D
Sallum, S., Follette, K. E. J., Close, L. M., et al. 2015, Natur, 527, 342
Sanchis, E., Picogna, G., Ercolano, B., et al. 2020, MNRAS, 492, 3440
Szulagyi, J., & Ercolano, B. 2020, arXiv:2002.09918v1
Thanathibodee, T., Calvet, N., Bae, J., et al. 2019, ApJ, 885, 94
Thanathibodee, T., Molina, B., Calvet, N., et al. 2020, ApJ, 892, 81
Uyama, T., Norris, B., Guyon, O., & Tamura, M. 2020, arXiv:2008.10780
Wagner, K., Follete, K. B., Close, L. M., et al. 2018, ApJL, 863, L8
Wang, J. J., Ginzburg, S., Ren, B., et al. 2020a, AJ, 159, 263
Wang, S., Kanagawa, K. D., Hayashi, T., & Suto, Y. 2020b, ApJ, 891, 166
Wu, Y.-L., Close, L. M., Eisner, J. A., et al. 2017b, ApJ, 836, 223
Wu, Y.-L., Sheehan, P. D., Males, J. R., et al. 2017a, ApJ, 836, 223
Zhang, S., Zhu, Z., Huang, J., et al. 2018, ApJL, 869, L47
Zhu, Z., Ju, W., & Stone, J. M. 2016, ApJ, 832, 193
Zurlo, A., Cugno, G., Montesinos, M., et al. 2020, A&A, 633, 119